Separation and Purification Technology 353 (2025) 128356

Contents lists available at ScienceDirect

Separation and Purification Technology

journal homepage: www.elsevier.com/locate/seppur

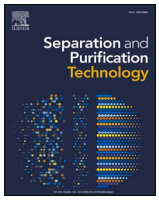

Fe-Ce based metal-organic framework as a novel heterogeneous catalyst accelerating redox cycle for efficient degradation of sulfamethoxazole in wide pH ranges

Shu-Ting Cheng, Jia-Xin Song, Li-Hong Yu, Xiao-Fang Shen, Yue-Hong Pang *

School of Food Science and Technology, Jiangnan University, Wuxi 214122, China

ARTICLE INFO

Editor: C. Han

Keywords:
Heterogeneous electro-Fenton
Degradation
Bimetallic catalyst
Sulfamethoxazole
Mineralization

ABSTRACT

The electro-Fenton (EF) technology holds immense potential for wastewater treatment. However, there persist certain factors that affect its degradation efficiency, such as the restricted pH range, production of iron sludge and sluggish conversion rate between Fe^{2+} and Fe^{3+}. Herein, 2,3,6,7,10,11-hexahydroxytriphenyl (HHTP) was introduced as the organic ligand to synthesize a series of efficient iron-based MOF catalysts (Fe_xCe_1-HHTP (x = 1, 2, 3, 4)) with different molar ratios for sulfamethoxazole (SMX) degradation in heterogeneous EF system. HHTP with electron-rich functional groups is beneficial to enhance performance of oxygen evolution reaction. Among these catalysts, Fe_3Ce_1-HHTP catalyst achieved 97.3 % degradation efficiency in 30 min and mineralization rate was 89.7 % at 1 h. The introduction of Ce promoted the transition of Fe^{3+} and Fe^{2+} in heterogeneous EF reaction. The synergistic effects between Fe^{3+}/Fe^{2+} and Ce^{4+}/Ce^{3+} further catalyzed the generation of hydroxyl radicals and it was proved as the main active species. The heterogeneous catalyst showed good performance in wide pH range, good stability, and high degradation efficiency to other pollutants. Three possible SMX degradation routes are suggested on basis of intermediates detected by mass spectrum analysis and theoretical calculations. The toxicity of these intermediates was assessed using Toxicity Estimation Software Tool (T.E.S.T.). This work provides valuable guidance for the design of highly efficient and stable heterogeneous EF catalyst for antibiotic degradation and expand the application potential in wastewater treatment of organic pollutants.

1. Introduction

Antibiotics have gained widespread usage worldwide due to their potent antibacterial properties and comparatively affordable cost, effectively supporting the health of humans, animals and plants [1,2]. However, irrational usage and even abuse of a large amount of antibiotics, incomplete absorption and metabolism after antibiotic ingestion, and unintentional discharge of wastewater by pharmaceutical companies and hospitals pose a serious threat to humans and aquatic ecosystems [3,4]. Traditional wastewater treatment technologies including adsorption [5], filtration [6], and biological methods [7] can only partially remove antibiotics. Therefore, developing an efficient method for eliminating antibiotics from wastewater is of great significance.

Recently, electro-Fenton (EF) technique has proven to be one of the most effective methods for antibiotic removal [8,9]. EF technology mainly generates H_2O_2 in situ at cathode, subsequently reacting with added Fe^{2+} to produce reactive oxide species (ROS), including hydroxyl radicals (·OH), thereby enhancing pollutants degradation [10]. EF technology does not require additional H_2O_2, avoiding the risks of H_2O_2 storage and transportation [11,12]. The consumed Fe^{2+} can be regenerated by continuous electro reduction of Fe^{3+}, which has been proven to be a promising approach to eliminate antibiotics [13]. Nevertheless, widespread practical application of traditional homogeneous Fenton process is still hindered by some drawbacks, such as limited acidic pH range and production of substantial iron hydroxide sludge [14,15]. The development of heterogeneous EF technology based on solid catalysts alleviates these problems to some extent [16,17]. For many catalysts, cycling efficiency of Fe^{2+}/Fe^{3+} is relatively low, and they may lose some of their active sites during degradation process, leading to the dissolution of excess iron [18]. Hence, it is significant for the development of efficient and stable heterogeneous EF catalyst.

Metal-organic frameworks (MOFs), characterized by their porosity, metal sites, and structural diversity, possess the ability to convert H_2O_2 into ·OH [19]. However, due to the poor electrical conductivity of

* Corresponding author.
E-mail address: yhpang@jiangnan.edu.cn (Y.-H. Pang).

https://doi.org/10.1016/j.seppur.2024.128356
Received 16 April 2024; Received in revised form 3 June 2024; Accepted 7 June 2024
Available online 13 June 2024

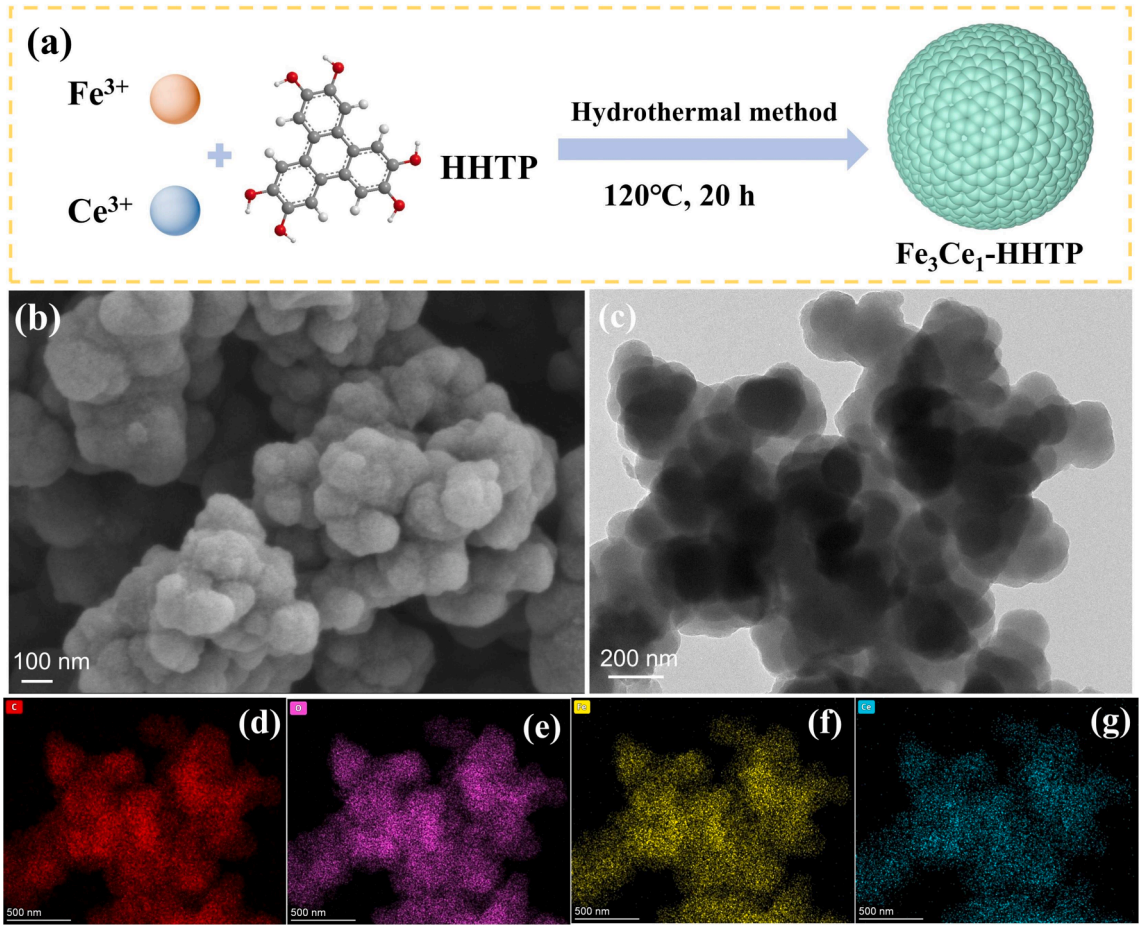

Fig. 1. (a) The synthesis of Fe_3Ce_1-HHTP catalyst; (b) SEM image and (c) TEM image of Fe_3Ce_1-HHTP; The elemental mapping images of (d) C, (e) O, (f) Fe, (g) Ce.

ligands around metal sites, most MOFs are restricted by the scarcity of open active sites, sluggish mass transfer, and high resistance, which limits the application in electro-catalysis [20,21]. 2,3,6,7,10,11-hexahydroxytriphenyl (HHTP) is a class of organic molecules that possess large ring structure and electron-rich functional groups [22,23]. The electron-rich functional groups can modulate electronic structure of metal active sites [24]. The conductive MOF material composed of HHTP as an organic ligand is rich in a large amount of oxygen element, which is beneficial for improving oxygen evolution reaction (OER) performance [25,26]. Additionally, there exist many unsaturated sites in MOF structure, which can bind other metal ions through coordination bonds [27]. Dong et al. synthesized a Ni-based conductive MOF (Ni-HHTP) that features numerous Ni^{3+} centers, which has a large electrochemical surface area and high intrinsic activity in OER [28]. Sun et al. fabricated Cu-HHTP as an active oxidation reduction reaction (ORR) electrocatalyst with high selectivity for H_2O_2 production [29]. Li et al. prepared $Cu_3(HHTP)_2$ to provide large active surface areas for catalytic oxidation, enhancing charge transfer efficiency in malachite green detection [30]. These properties of HHTP have great potential in Fenton reaction systems. However, few studies have been reported on the utilization of HHTP ligand-based MOF in heterogeneous EF degradation.

In this work, Fe_xCe_1-HHTP (x = 1, 2, 3, 4) catalysts were prepared by hydrothermal synthesis, incorporating the organic ligand HHTP. Sulfamethoxazole (SMX), a representative broad-spectrum sulfonamide antibiotic, was chosen as a target contaminant to estimate degradation efficiency. HHTP with electron-rich functional groups offers possibility for satisfactory SMX degradation performance. Ce could effectively accelerate electron transfer rate, which was beneficial for H_2O_2 production. The prepared iron-based MOF catalyst in heterogeneous EF system can facilitate the redox cycling of Fe^{3+}/Fe^{2+} and Ce^{4+}/Ce^{3+}. The synergistic effect of bimetals significantly improves the catalytic performance and achieves high efficiency mineralization rate. This study aims to prepare a novel and efficient heterogeneous EF catalyst for effective degradation of organic pollutants and broaden its application in water treatment.

2. Materials and methods

2.1. Materials

Details of the reagents and experimental materials are provided in **Text S1** of Supporting Information.

2.2. The synthesis of Fe_xCe_1-HHTP (x = 1, 2, 3, 4)

The Fe_xCe_1-HHTP (x = 1, 2, 3, 4) was synthesized by mixing $FeCl_3{\cdot}6H_2O$ and $Ce(NO_3)_3{\cdot}6H_2O$ with different molar ratios, 1.25 mM HHTP and 30 mL DMF, stirring for 30 min until completely dissolved. The solution was transferred to a 50 mL Teflon-lined stainless steel container, reacting at 120℃ for 20 h. The deposit was separated by centrifugation and thoroughly washed with DMF and ethanol, each three times. The total number of molars of iron and cerium was 5 mM, different molar ratios of Fe_xCe_1-HHTP (x = 1, 2, 3, 4) catalysts were synthesized. The synthesis of Fe-HHTP followed the same protocol, excluding the addition of $Ce(NO_3)_3{\cdot}6H_2O$.

2.3. Characterizations

The characterizations of prepared catalysts are shown in **Text S2** of Supporting Information.

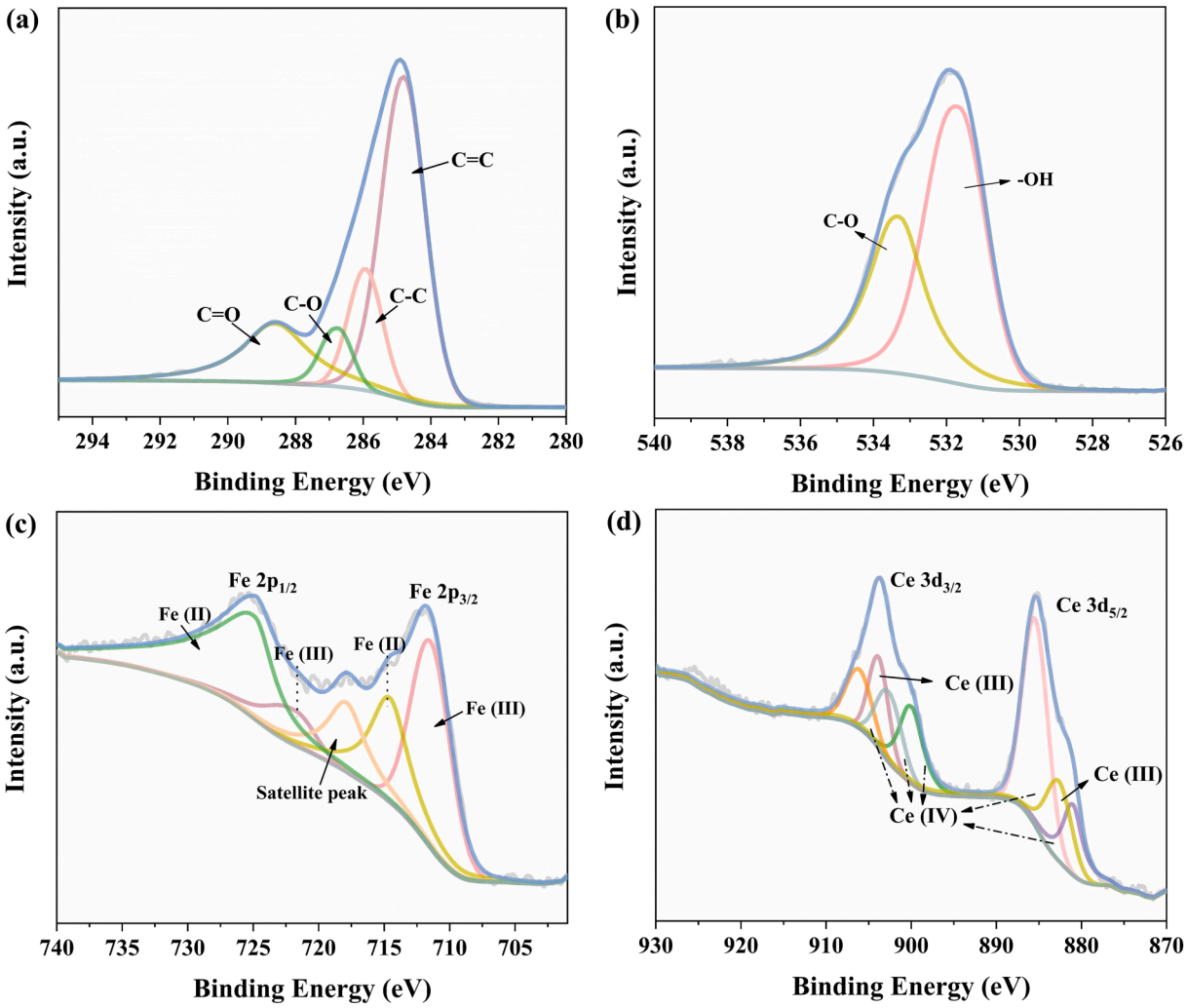

Fig. 2. XPS spectra of Fe_3Ce_1-HHTP: (a) C 1 s; (b) O 1 s; (c) Fe 2p and (d) Ce 3d.

2.4. The heterogeneous EF degradation

The simulated wastewater was SMX aqueous solution (10 mg/L, 100 mL) containing 0.05 M Na_2SO_4 electrolyte under constant current conditions. The cathode was carbon cloth, the anode was platinum sheet, and their distance measured 2 cm. Prior to heterogeneous EF degradation, Fe_xCe_1-HHTP (x = 1, 2, 3, 4) catalyst dispersed in solution by stirring for 10 min to get adsorption equilibrium. Meanwhile, O_2 was bubbled into the solution (0.6 L/min) to establish a stable oxygen environment. The heterogeneous EF reaction was initiated when the DC power supply was turned on. Samples were collected with syringes at different times and subsequently filtered through 0.22 μm microporous filter membranes. In cycle experiment, catalyst was collected by centrifuge and dried at 60℃ for reuse. Detailed methods for detecting SMX are shown in **Text S3**.

2.5. Analytical methods

Total organic carbon (TOC, Multi N/C 3100, Jena, Germany) was used to analyze the mineralization efficiency of the whole SMX degradation process. The Fe and Ce concentrations in solution were determined using an inductively coupled plasma mass spectrometry (ICP-MS, Agilent 7800, USA). Three-dimensional excitation-emission matrix fluorescence spectra (3D EEMs) were acquired by a fluorescence spectrophotometer (Hitachi, F7000). The detailed of H_2O_2 experiment is shown in **Text S4**. Density functional theory (DFT) was used to calculate and predict the vulnerable sites of SMX, detailed information is shown in **Text S5**. The degradation intermediates were determined using mass spectrometry (MS, QTRAP 4500, AB SCIEX, USA). The toxicity of SMX and its intermediates was predicted by Toxicity Estimation Software Tool (T.E.S.T.).

3. Results and discussion

3.1. The characterizations of catalyst

The preparation of Fe_3Ce_1-HHTP catalyst is exhibited in Fig. 1**a**. The morphology of Fe_3Ce_1-HHTP was characterized by scanning electron microscope (SEM) (Fig. 1**b**) and transmission electron microscopy (TEM) (Fig. 1**c**). Fe_3Ce_1-HHTP showed uniform size of nanocluster with rough surface, enhancing electron transfer and mass diffusion to accelerate the heterogeneous EF reaction. Meanwhile, energy dispersive spectrometer elemental mapping demonstrated that C, O, Fe, and Ce elements are uniformly distributed on the catalyst (Fig. 1**d-g**), indicating the successful synthesis of Fe_3Ce_1-HHTP.

C 1 s spectrum, as shown in Fig. 2**a**, exhibited four peaks at 284.8, 285.9, 286.8 and 288.6 eV, which corresponded to C = C, C–C, C-O and C = O [31]. The spectrum of O 1 s consists mainly of peaks with binding energies of 531.8 and 533.4 eV (Fig. 2**b**). These peaks were attributed to the ·OH species which facilitated the electrocatalytic reaction and C-O bond [32,33]. For Fe 2p spectra, the peaks observed at 711.8 and 724.9 eV represented Fe $2p_{3/2}$ and Fe $2p_{1/2}$, respectively (Fig. 2**c**).

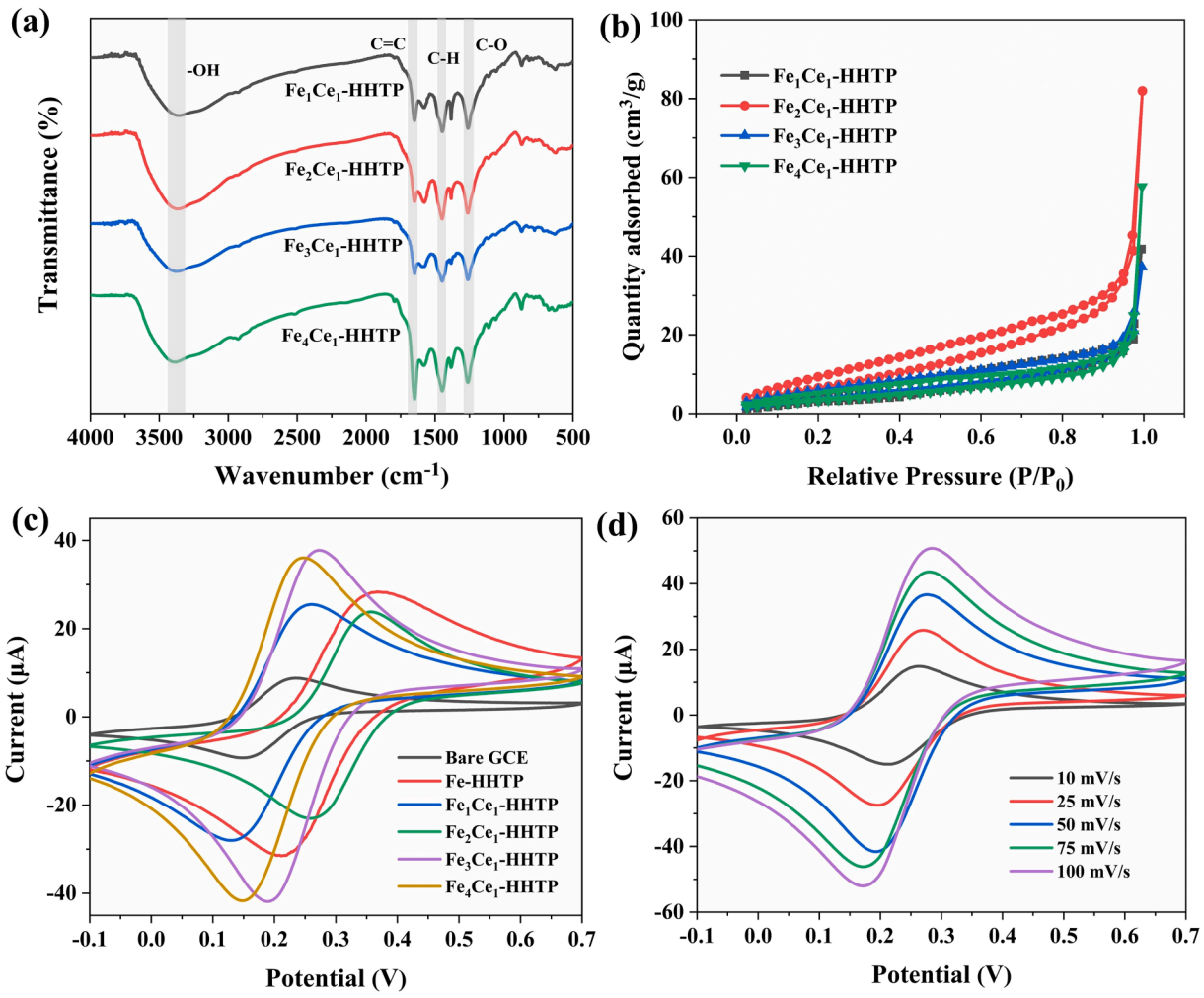

Fig. 3. (a) FT-IR spectra and (b) N_2 adsorption–desorption isotherms of Fe_xCe_1-HHTP (x = 1, 2, 3, 4); (c) CV curves of different modified GCE; (d) CV curves of Fe_3Ce_1-HHTP at different scan rates.

Additionally, two peaks at 711.6 and 721.8 eV were corresponded to Fe (II), the peaks at 714.7 and 725.2 eV were attributed to Fe (III), respectively [34,35]. Additionally, a satellite peak was observed at 718.1 eV, situated between Fe $2p_{3/2}$ and Fe $2p_{1/2}$. The Ce 3d spectra were resolved into two main peaks, representing Ce $3d_{5/2}$ at 885.2 eV and Ce $3d_{3/2}$ at 903.7 eV (Fig. 2**d**). In addition, the pattern of Ce 3d comprised seven peaks, which represented the binding energies of Ce (III) (882.7 and 903.9 eV) and Ce (IV) (881.1, 885.6, 900.2, 902.9 and 906.3 eV) [36]. In addition, full scan spectrum of Fe_3Ce_1-HHTP and Fe-HHTP is shown in **Fig. S1**, further indicating the successful synthesis of bimetals.

The surface functional groups of the synthesized catalysts were characterized by Fourier-transform infrared spectrometer (FT-IR) analysis. Fig. 3**a** shows a typical FT-IR spectrum of different metal ratios of Fe_xCe_1-HHTP (x = 1, 2, 3, 4). The broad peak at 3392 cm^{-1} was ascribed to stretching vibration of hydroxyl groups in adsorbed water molecules [37]. The infrared spectra of Fe_xCe_1-HHTP showed distinct absorption peaks at 1259, 1450 and 1650 cm^{-1}, corresponding to characteristic vibrations of C-O, C–H and C = C bonds, within benzene ring of organic ligand HHTP, respectively [38]. FT-IR spectra of Fe_xCe_1-HHTP (x = 1, 2, 3, 4) catalysts showed no significant changes except for the peak intensity. In **Fig. S2**, powder X-ray diffraction (PXRD) pattern of prepared catalyst showed the obvious crystalline structure.

The N_2 adsorption–desorption isotherms and pore size distribution of Fe_xCe_1-HHTP (x = 1, 2, 3, 4) with different molar amount of metal are exhibited in Fig. 3**b** and **Fig. S3**. High specific surface area generally means excellent catalytic performance. However, Fe_3Ce_1-HHTP with lower surface area showed better degradation efficiency than the other catalysts, which indicated the contribution of increasing surface area to pollutant removal was negligible. The specific surface area and pore volume of Fe_3Ce_1-HHTP were slightly decreased compared to other catalysts, which was corresponding to the adsorption effect of different metal contents in 10 min. These catalysts exhibited a range of 3–10 nm pore size distribution. It was calculated that the molecular diameter of SMX is about 14.9 Å (**Fig. S4**). Therefore, among these prepared catalysts, Fe_3Ce_1-HHTP with pore size distribution of 3.7 nm was more suitable, which was closer to the size of SMX.

Cyclic voltammetry (CV) test evaluated conductivity of Fe_xCe_1-HHTP (x = 1, 2, 3, 4) catalysts with different metal ratios. In Fig. 3**c**, the peak current of electrode modified catalyst was significantly enhanced compared to the bare GCE, Fe_3Ce_1-HHTP showed higher electrochemical activity. Furthermore, CV curves of Fe_3Ce_1-HHTP with different sweep rates are exhibited in Fig. 3**d**, the peak current showed a linear relationship with the square root of scanning rate the scan rate (**Fig. S5**), demonstrating the redox reaction on Fe_3Ce_1-HHTP catalyst was diffusion-controlled [20,39]. These results indicated that Fe_3Ce_1-HHTP exhibited faster electron transfer rate.

3.2. *Degradation performance of SMX in EF system*

SMX was selected for a target antibiotic to investigate the degradation efficiency of fabricated catalyst. SMX degradation under different

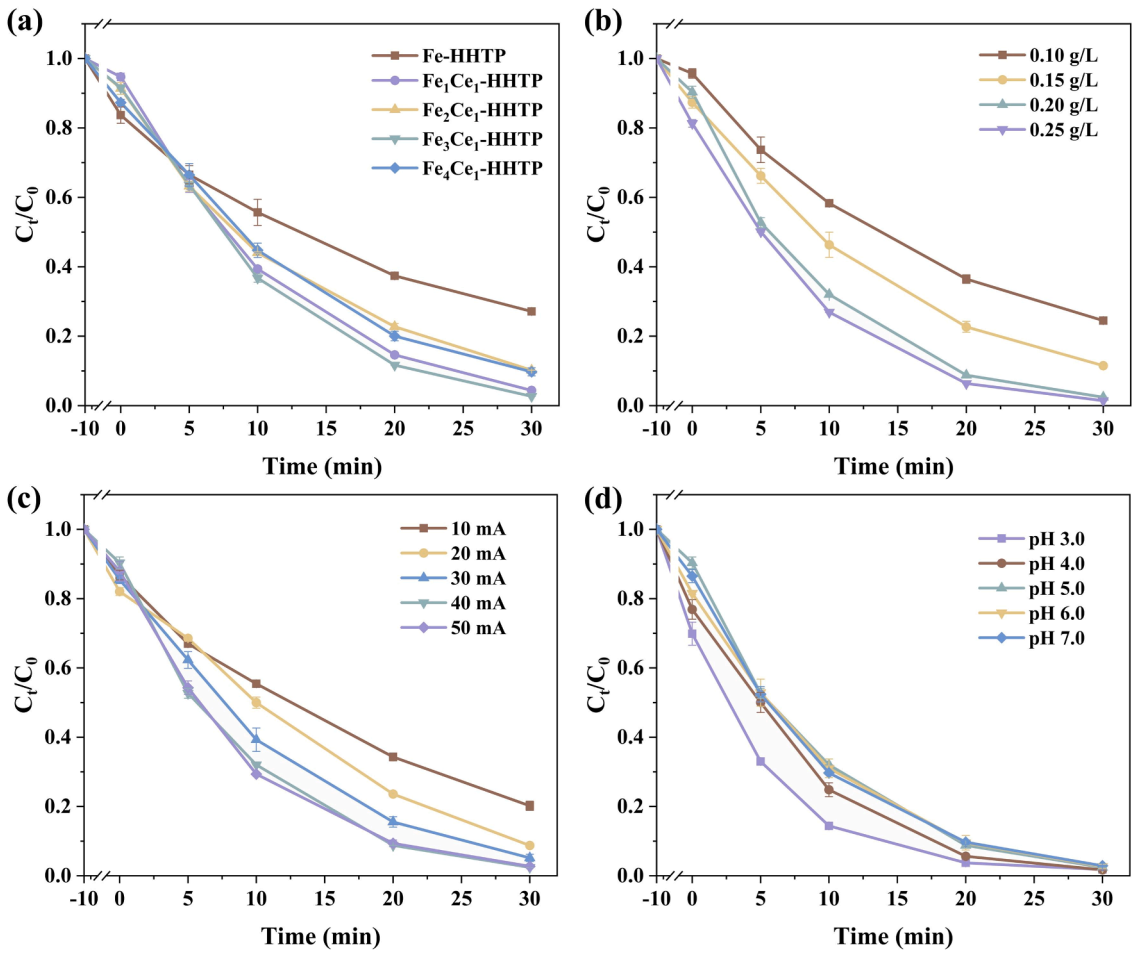

Fig. 4. The effect of (a) Fe/Ce ratio; (b) the catalyst dosage; (c) current and (d) initial pH on the heterogeneous EF performance. (Conditions: [initial SMX concentration] = 10 mg/L, [catalyst dosage] = 0.20 g/L, [current] = 40 mA, [initial pH] = 5.0).

conditions are exhibited in Fig. S6. SMX degradation efficiency was only 10 % by adsorption without current, 26.1 % for anodic oxidation. In contrast, 97.3 % SMX could be degraded in 30 min by heterogeneous EF reaction.

The introduction of different molar ratios of Fe and Ce can not only effectively adjust the metal content in the composite, but also significantly improve the conductivity of the catalyst, thus optimizing the electrocatalytic performance. Fe_xCe_1-HHTP (x = 1, 2, 3, 4) catalysts with different metal contents were prepared by adjusting the concentrations of $FeCl_3{\cdot}6H_2O$ and $Ce(NO_3)_3{\cdot}6H_2O$ and the integral molar quantity was 5 mM. In Fig. 4**a**, SMX degradation efficiency obtained with Fe_1Ce_1-HTTP, Fe_2Ce_1-HTTP, Fe_3Ce_1-HTTP and Fe_4Ce_1-HTTP was 95.6 %, 89.8 %, 97.3 % and 90.3 %, respectively. Compared with the undoped cerium catalyst Fe-HTTP (72.9 %), SMX degradation rate of Fe_3Ce_1-HTTP was significantly enhanced by 24.4 %. The introduction of Ce enhanced availability of catalytic active sites and reacted with iron ions, facilitating the interaction of catalyst and H_2O_2 to generate ·OH, thus enhancing the oxidative degradation process.

In Fig. 4**b**, the degradation rate greatly improved from 75.5 % to 97.6 % in 30 min when the catalyst dosage was increased from 0.10 to 0.20 g/L. The corresponding reaction rate constants of catalyst dosage at 0.10, 0.15, 0.20 and 0.25 g/L were 0.045, 0.069, 0.121 and 0.136 min^{-1} (Fig. S7). The increased catalyst provided more active sites for adsorption and H_2O_2 activation, leading to production of abundant ·OH that facilitated SMX degradation [40]. Nevertheless, further increasing catalyst dosage to 0.25 g/L did not accelerate the degradation process obviously, possibly due to the inhibiting effect of excessive iron sites reacting with ·OH, hindering the EF reaction. Therefore, 0.20 g/L catalyst was used for subsequent experiments.

In Fig. 4**c**, the degradation of SMX exhibited a consistent upward trend as current increased from 10 to 40 mA, achieving 97.6 % SMX removal at 40 mA. Simultaneously, the reaction rate constant increased from 0.048 to 0.121 min^{-1}, a 2.52-fold increase (Fig. S8). Then the degradation rate declined to 97.3 % slightly with increasing current to 50 mA. It implied that the sufficient current was beneficial for enhancing electron transfer, excessive current led to the conversion of O_2 to H_2O by the $4e^-$ pathway of ORR, rather than forming H_2O_2 via the $2e^-$ pathway [20,41]. As shown in Fig. S9**a**, H_2O_2 concentration increased with the increase of current intensity and it could accumulate up to 66.4 mg/L within 30 min at 40 mA. In Fig. S9**b**, the current efficiency ranged from 48.9 % to 55.3 %. In addition, the electric energy consumption (EEC) for H_2O_2 generation was calculated to evaluate whether it can be applied on a large scale or not. EEC values ranged from ranged between 8.7 and 13.4 kWh/kg (Fig. S10), indicating the EF reaction requires lower energy consumption and is more conducive to efficient production of H_2O_2 [42,43]. Although the removal rate of SMX was almost the same at 40 mA and 50 mA, the EEC was lower at 40 mA. Considering the both degradation effect and energy consumption, 40 mA was determined to be optimal current for this experiment.

The pH effect of SMX degradation ranging from 3.0 to 7.0 was investigated in Fig. 4**d**, and degradation rates were between 97.1 % and 98.3 %, indicating that the wide pH range in application of Fe_3Ce_1-HTTP based EF degradation system. The reaction rate constant ranged between 0.114 and 0.131 min^{-1}, and there is almost no difference within the tested pH range (Fig. S11). This suggests a broad pH application window for the catalyst. Considering the proportion of adsorption and

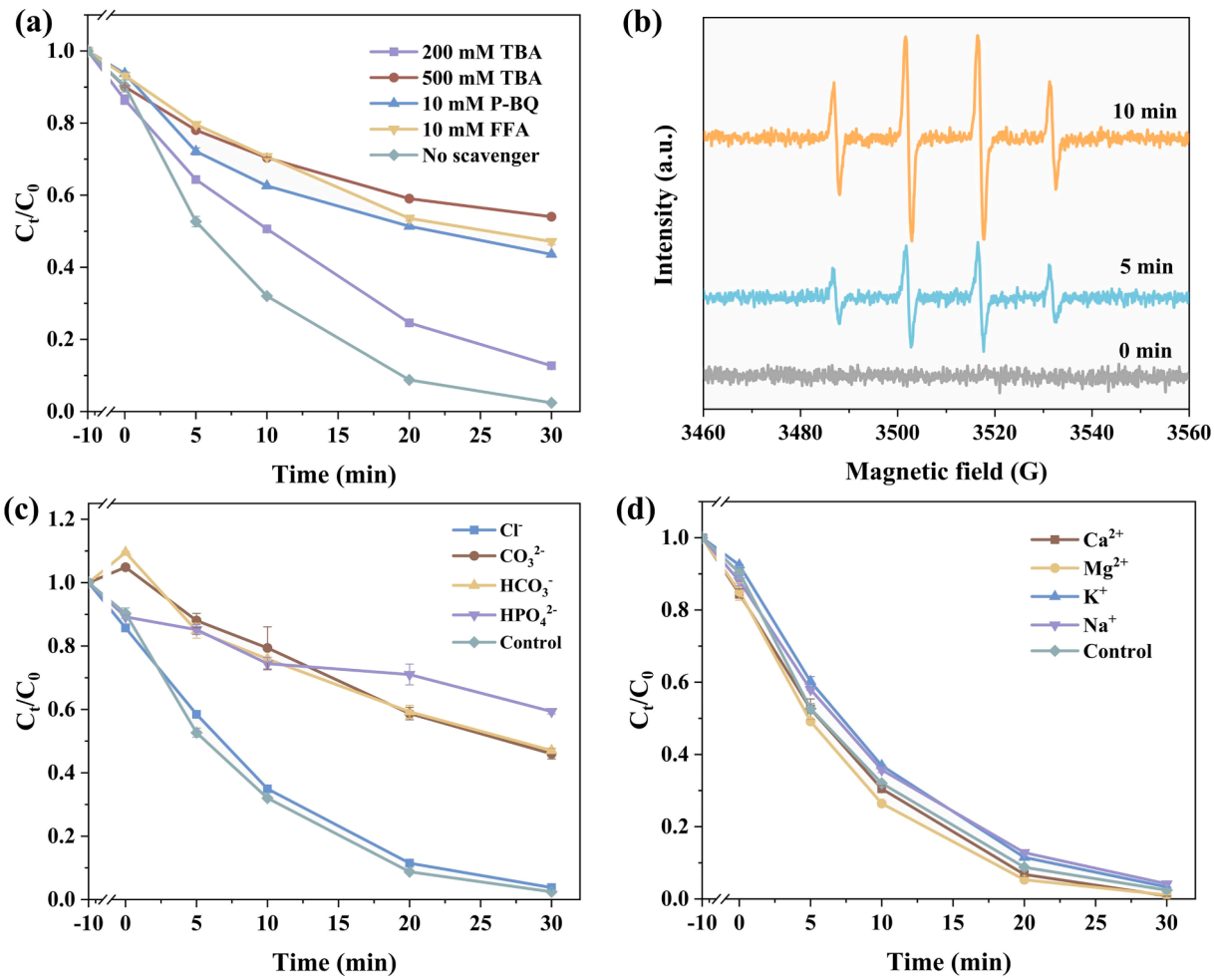

Fig. 5. (a) Free radical trapping experiment with the addition of different scavengers; (b) EPR spectra at different interval of ·OH; The effect of (c) inorganic anions and (d) metal ions for SMX degradation.

the reaction between metal and acid was faster in the strongly acidic system, the metal was easily dissolved [44], pH 5.0 was selected to conduct the subsequent experiment.

3.3. Degradation mechanism of SMX in EF system

To investigate degradation mechanism of Fe_3Ce_1-HTTP, free radical quenching experiment was carried on to determine types of ROSs

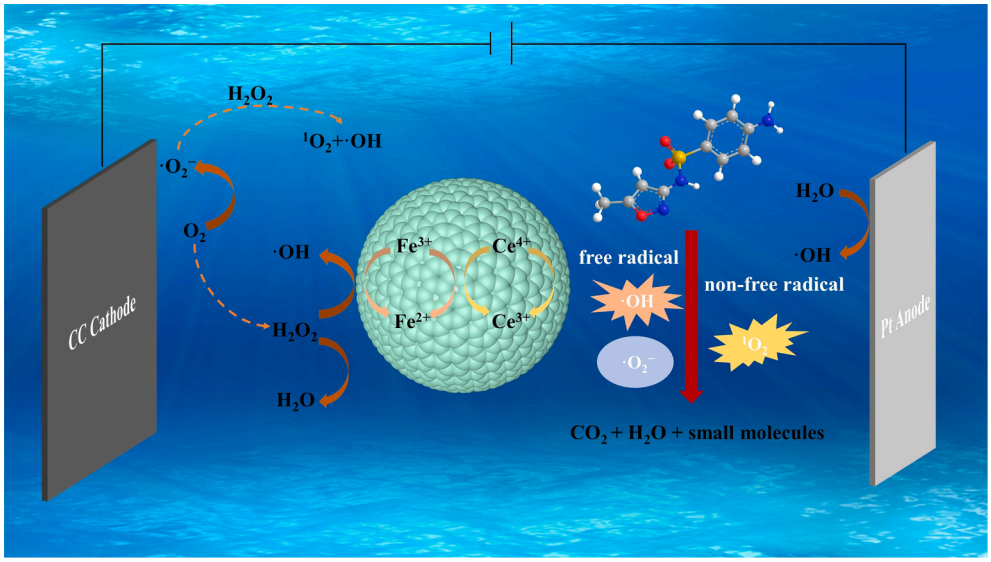

Fig. 6. The SMX degradation mechanism of heterogeneous EF process with Fe_3Ce_1-HHTP catalyst.

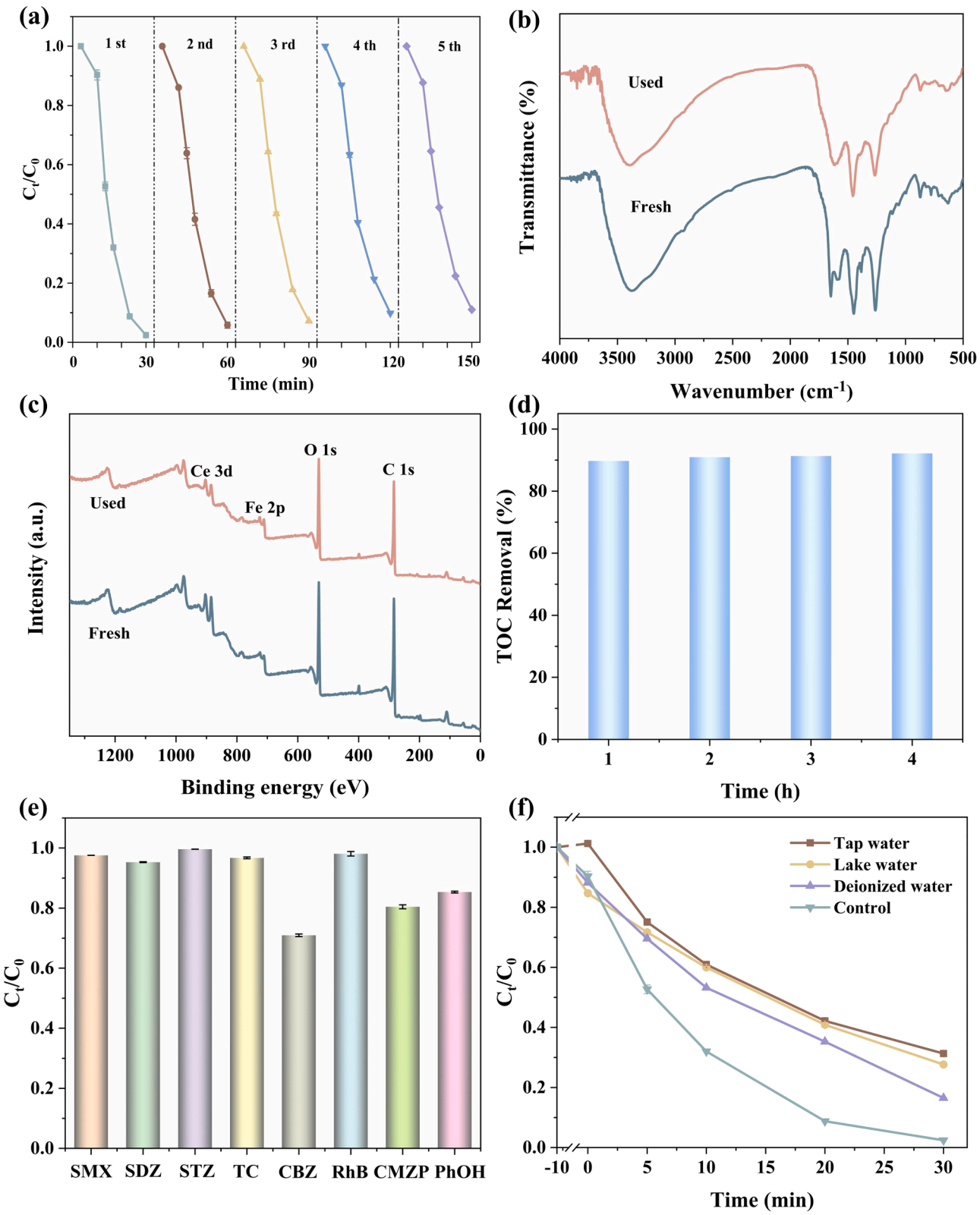

Fig. 7. (a) Reusability of Fe_3Ce_1-HHTP catalyst for five runs with under the same conditions; (b) FT-IR and (c) XPS spectra of fresh and used Fe_3Ce_1-HHTP catalyst; (d) TOC removal efficiency of Fe_3Ce_1-HHTP catalyst; (e) Degradation of different organic pollutants by the heterogeneous EF system; (f) SMX degradation efficiency in different real water. (Conditions: [initial SMX concentration] = 10 mg/L, [catalyst dosage] = 0.20 g/L, [current] = 40 mA, [initial pH] = 5.0).

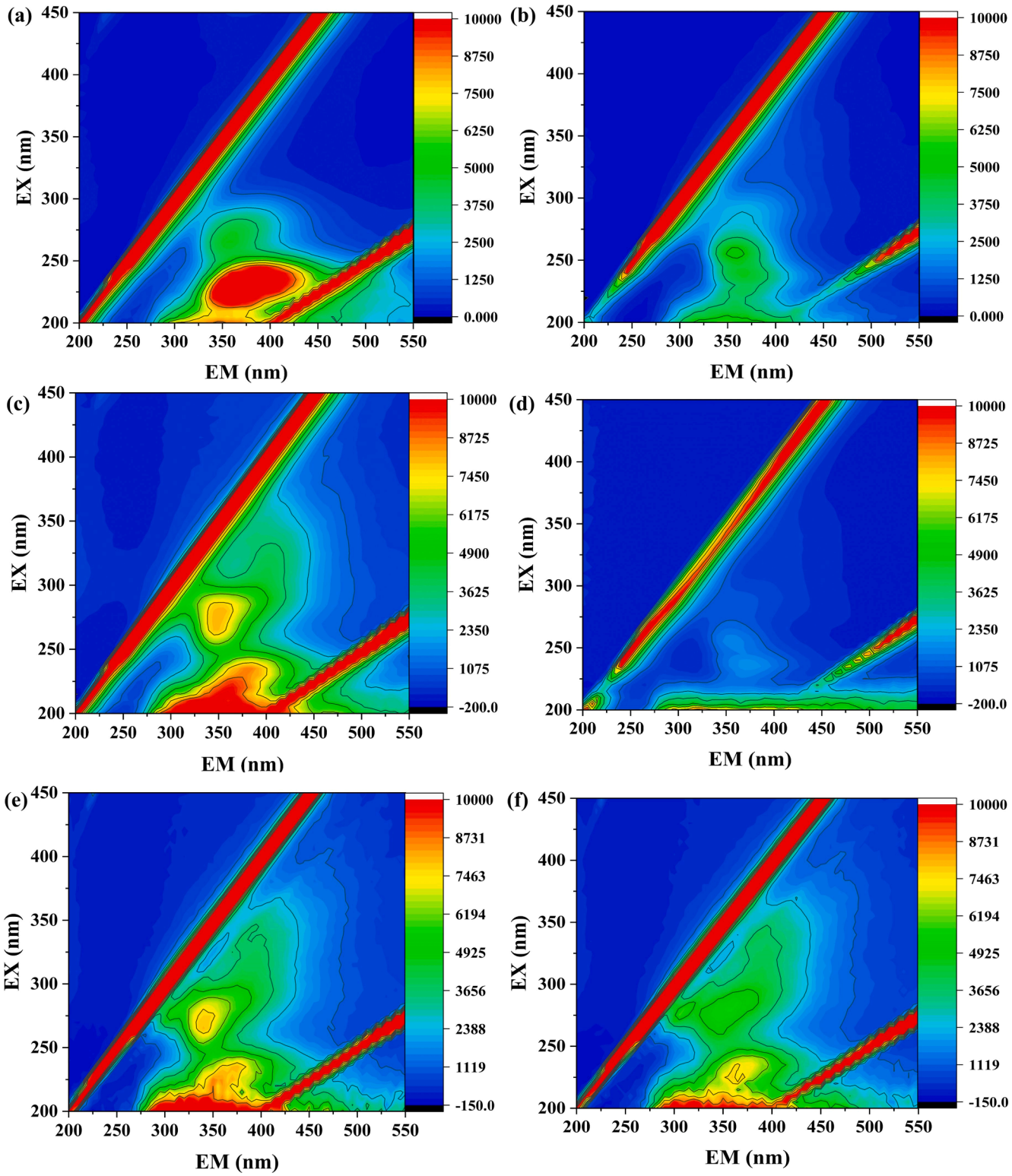

Fig. 8. Fluorescence 3D EEMs spectra of tap water: (a) 0 min and (b) 30 min; deionized water: (c) 0 min and (d) 30 min; lake water: (c) 0 min and (d) 30 min in EF process with Fe_3Ce_1-HHTP.

involved in SMX degradation system. In Fig. 5**a**, *tert*-butanol (TBA), p-benzoquinone (p-BQ) and furfuryl alcohol (FFA) were the scavengers for ·OH, $\cdot O_2^-$ and $^1O_2$ radicals [45], respectively. SMX was nearly removed within 30 min without adding any scavenger. When 200 mM TBA was introduced into the system, SMX removal rate only decreased by 10.3 %, and SMX degradation decreased significantly to 46 % in introduction of 500 mM TBA.

After introduction of 10 mM p-BQ and FFA, SMX removal rate decreased to 56.4 % and 52.8 % at 30 min. These results showed that ·OH, $\cdot O_2^-$ and $^1O_2$ all participate in SMX degradation, and ·OH was main active oxygen species. To further confirm the ·OH production, electron paramagnetic resonance (EPR) experiment was carried out with DMPO as trapping agent [46]. The EPR signal exhibiting intensity ratio of 1:2:2:1 was characteristic signal of DMPO-·OH (Fig. 5**b**). As the reaction

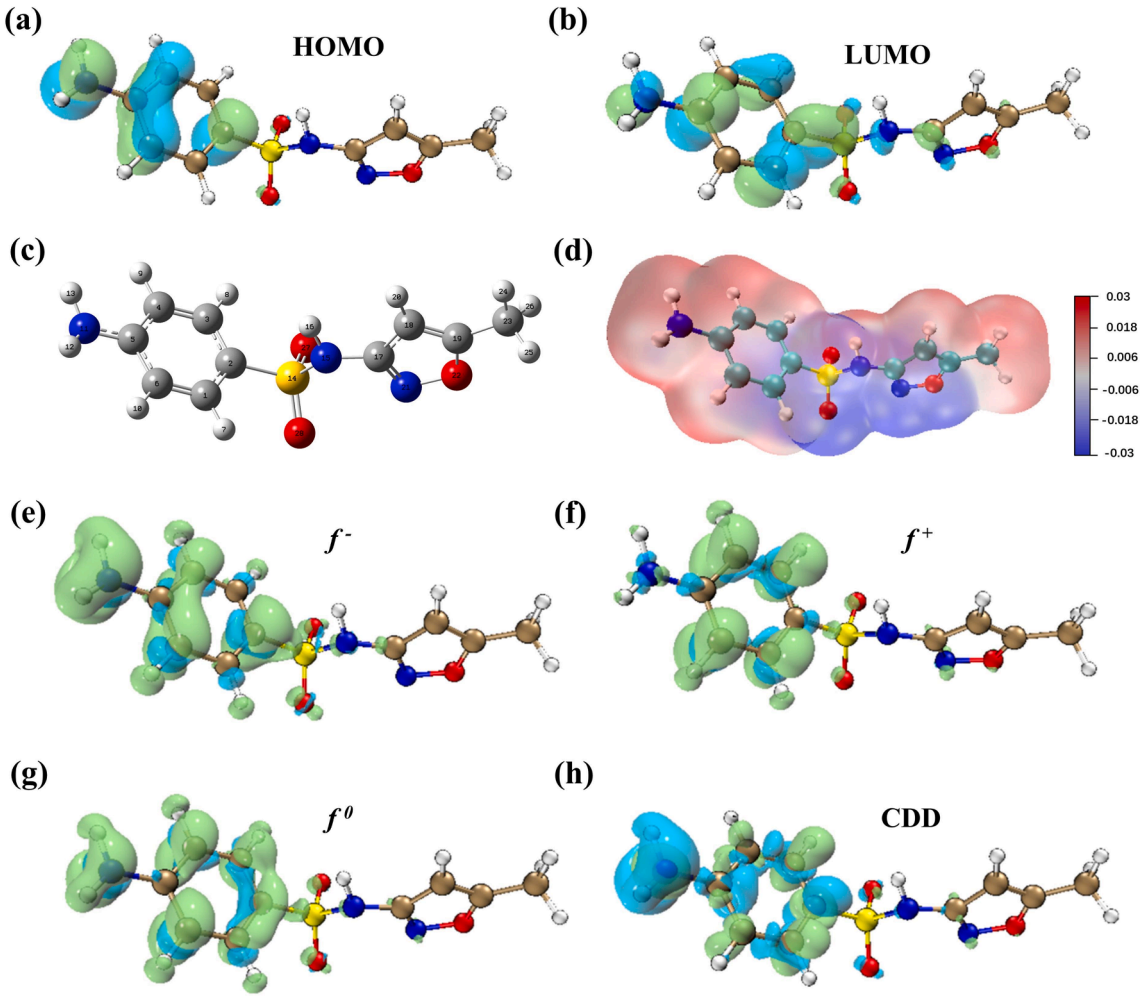

Fig. 9. (a) HOMO; (b) LUMO; (c) The optimized SMX molecular structure; (d) ESP distribution map of SMX; The isosurface of condensed Fukui function of SMX: (e) f^-; (f) f^+; (g) f^0 and (h) CDD.

time prolonged, the signal intensity also increased, indicating the continuous generation of ·OH.

Various inorganic anions and metal ions exist in actual wastewater, which can potentially influence both the in-situ formation of H_2O_2 and SMX degradation performance [47]. In Fig. 5**c**, within 30 min of EF treatment, only 10 mM Cl^- was favorable for SMX degradation compared to the control group. Cl^- could be oxidized by ·OH, forming chlorine with lower activity than ·OH radical (Eqs. (S1) and (S2)) [36], which also participated in oxidative degradation. However, 10 mM HCO_3^- and CO_3^{2-} resulted in significant decreases in SMX degradation rate to 53 % and 54 %, respectively. This is attributed to the formation of lower potential $CO_3^{\cdot-}$ after the reaction of HCO_3^- (Eq. (S3)) [48] and the consumption of ·OH by these anions (Eq. (S4)). In addition, the introduction of 10 mM HPO_4^{2-} significantly inhibited the degradation (40.7 %), mainly owing to slow reaction rate of HPO_4^{2-} with ·OH to form a weak oxidizer ($HPO_4^{\cdot-}$) that is ineffective in oxidizing SMX (Eq. (S5)) [49]. On the other hand, as shown in Fig. 5**d**, metal ions such as Ca^{2+}, Mg^{2+}, K^+ and Na^+ had almost no impact on SMX degradation, with degradation rates remaining between 95.8 % and 99.1 %, indicating the proposed EF degradation process was not interfered by metal ions.

The possible mechanism of SMX degradation is shown in Fig. 6. Initially, a small portion of organic molecules in solution can be adsorbed onto Fe_3Ce_1-HHTP catalyst via electrostatic attraction or through interactions with functional groups. For EF process, O_2 dissolved in the solution is adsorbed on Fe_3Ce_1-HHTP catalyst and cathode, which are further converted into $\cdot O_2^-$ via one-electron ORR pathway or H_2O_2 during the two-electron ORR process (Eqs. (S6) and (S7)). Subsequently, H_2O_2 reacts with $\cdot O_2^-$ or Fe^{2+} to form ·OH radicals, and Fe^{3+} obtained electrons to regenerate Fe^{2+}, completing a cyclic redox reaction between Fe^{3+} and Fe^{2+} (Eqs. (S8) ~ (S11)). This cycle continuously generates active oxygen species, driving the degradation of organic pollutants. The generated $\cdot O_2^-$ reacts with H_2O_2 and ·OH to generate $^1O_2$ (Eqs. (S12) and (S13)). Additionally, Fe_3Ce_1-HHTP catalyst could effectively provide Ce^{4+}/Ce^{3+} redox pairs (Eqs. (S14) ~ (S16)). Therefore, Fe^{3+}/Fe^{2+} and Ce^{4+}/Ce^{3+} redox cycles could promote generation of active species including ·OH, $\cdot O_2^-$ and $^1O_2$. These ROSs diffused into the solution and participated in SMX degradation. Finally, SMX was mineralized into CO_2, H_2O and other small molecules (Eqs. (S17)).

3.4. Recyclability and applicability of catalyst

The degradation efficiency of catalyst gradually decreased after being reused for 5 times, which may be owing to occupancy of active catalyst sites by organic matter and loss of active metal components during EF process. The SMX degradation efficiency still remained 88.9 % within 30 min (Fig. 7**a**). Moreover, FT-IR, X-ray photoelectron spectroscopy (XPS) of Fe_3Ce_1-HHTP were compared before and after use, these characterizations exhibited the groups or characteristic peaks of catalyst did not change significantly and remained relatively stable (Fig. 7**b, c**). In **Fig. S12**, the XRD pattern and SEM image of Fe_3Ce_1-HHTP after the cycle experiment have almost no change, which provides great advantages for its long-term application. In **Fig. S13**, the dissolved

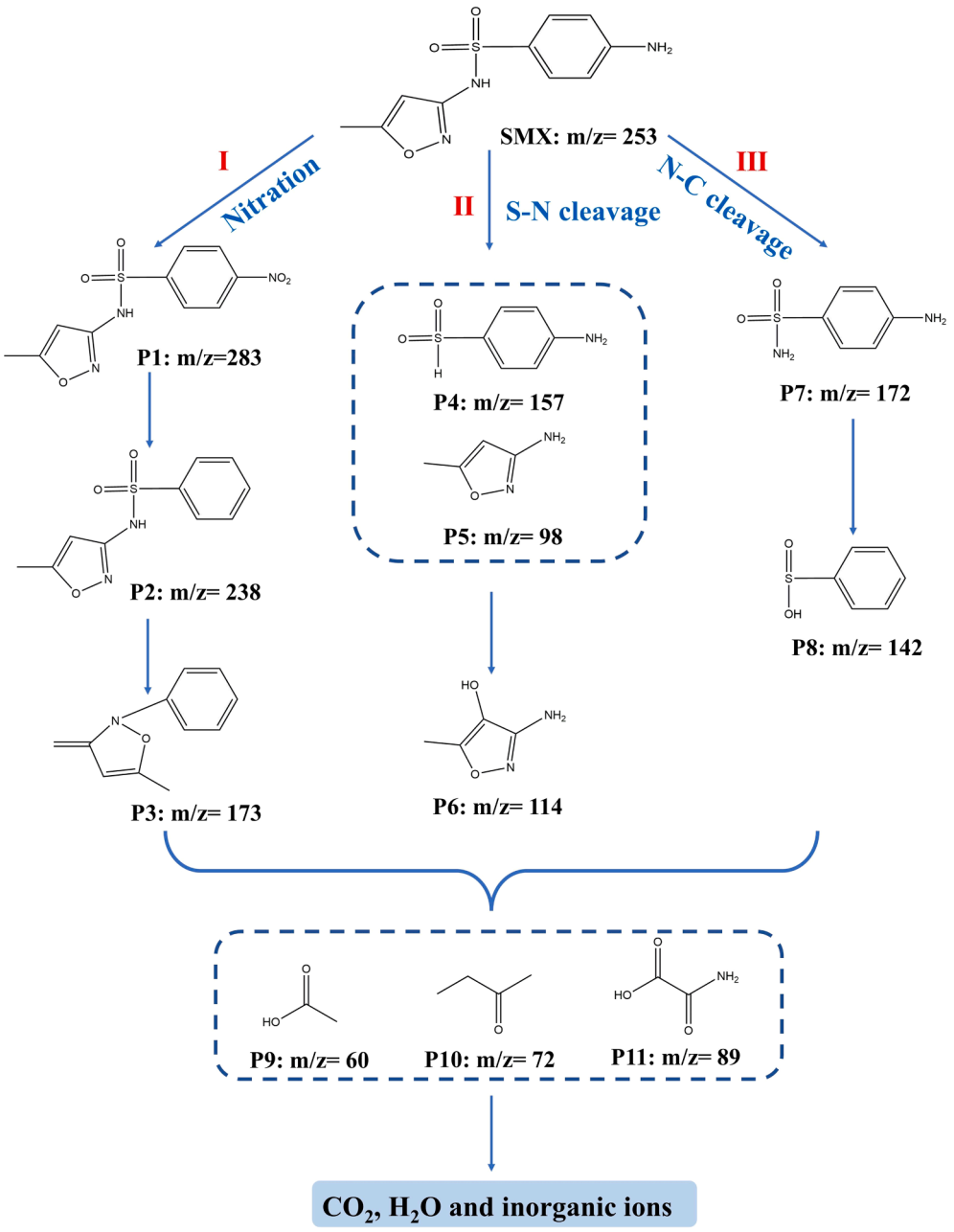

Fig. 10. The possible degradation pathway for SMX degradation by Fe_3Ce_1-HHTP catalyst.

iron concentration measured at 10 min and 30 min was 0.41 and 0.65 mg/L, which was lower than limit of 2 mg/L specified by the Chinese National Standard (GB 25467–2010). Ce concentration measured at 10 min and 30 min was 0.64 and 0.96 mg/L. Furthermore, Fe and Ce concentration measured after recycling experiment was 0.27 and 0.39 mg/L (Fig. S14). These results indicated that Fe_3Ce_1-HTTP had good stability and reusability.

TOC removal rate can reveal mineralization extent of pollutants to further evaluate degradation ability of the catalyst. In Fig. 7**d**, TOC removal rate reached 89.7 % within 1 h, achieving a relatively satisfactory result. The removal efficiency of TOC increased slowly over time, reaching 92.2 % after 4 h, indicating that the mineralization effect of SMX was excellent and most of the small molecular organic matter had been effectively mineralized, attributing to the effective conversion of H_2O_2 to ·OH by Fe_3Ce_1-HHTP catalyst. Comparisons of SMX degradation performance with other previously reported catalysts are shown in Table S2, Fe_3Ce_1-HHTP catalyst showed better degradation rate and mineralization effect, and shorter degradation time.

In order to investigate the degradation property of other pollutants, sulfadiazine (SDZ), sulfathiazole (STZ), tetracycline (TC), carbendazim (CBZ), rhodamine B (RhB) carbamazepine (CMZP) and phenol (PhOH) were introduced to heterogeneous EF process with same reaction conditions. Fig. 7**e** showed that degradation rates of Fe_3Ce_1-HTTP to various organic pollutants were 95.3 %, 99.6 %, 96.7 %, 71.0 %, 98.1 %, 80.5 % and 85.3 % within 30 min, respectively, which proved the effectiveness of Fe_3Ce_1-HTTP catalyst in degrading a variety of pollutants in EF system.

To evaluate performance of practical application, SMX degradation by Fe_3Ce_1-HHTP catalyst in heterogeneous EF process was studied by tap water, lake water and deionized water as aqueous substrates (Fig. 7**f**). The SMX removal rates were 68.7 %, 72.3 % and 83.5 % in 30 min, respectively. The SMX concentration increased after 10 min adsorption in tap water. Combined with the previous ion interference experiment, it indicated that there were some CO_3^{2-} and HCO_3^- in tap

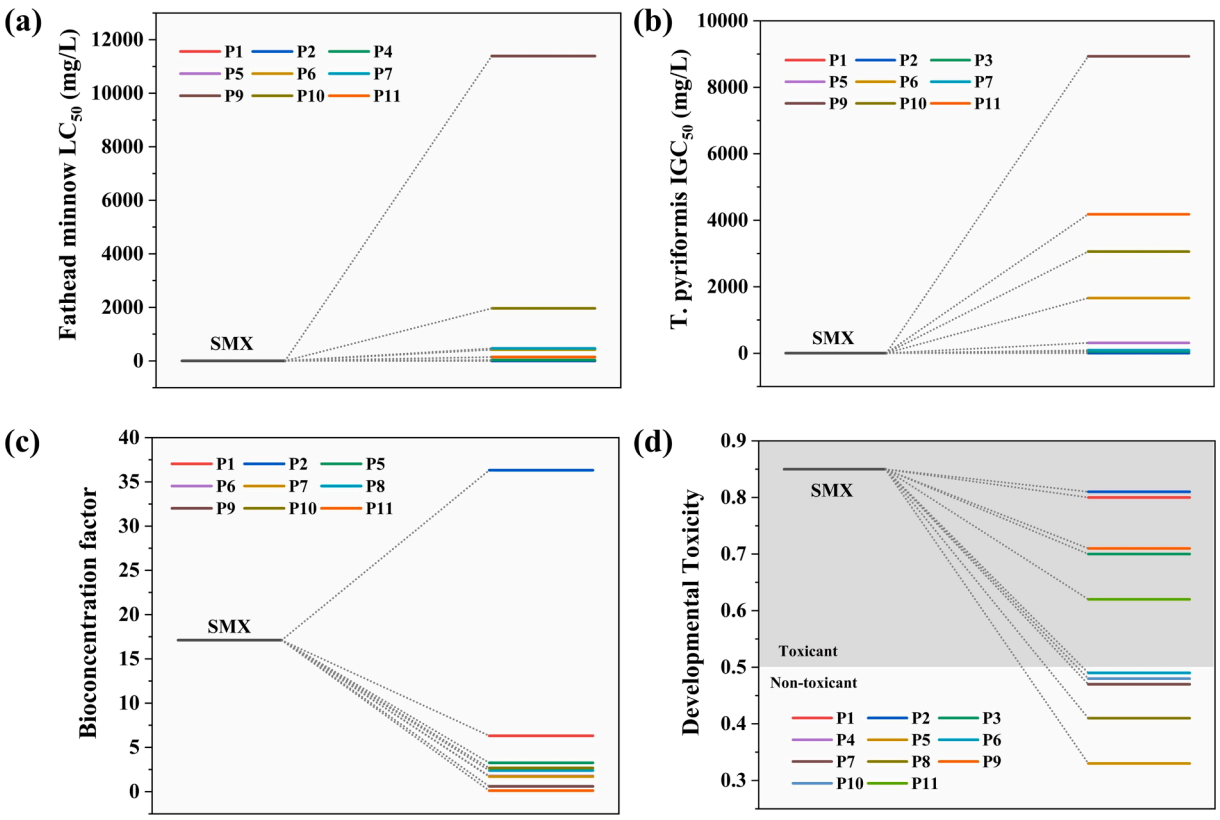

Fig. 11. (a) Fathead minnow LC_{50}; (b) T. pyriformis IGC_{50}; (c) bioaccumulation factor and (d) development toxicity of SMX and its degradation intermediates.

water, which inhibited SMX degradation effect to some extent.

To further demonstrate the degradation efficiency of SMX, 3D EEMs were performed with tap water, lake water and deionized water samples before and after 30 min degradation (Fig. 8). The fluorescence response region represented aromatic protein organoids in Ex/Em region of (200–320) nm/ (280–450) nm before degradation reaction [50]. With extension of degradation time, fluorescence intensity decreased significantly after 30 min, confirming that SMX was continuously degraded and eventually into small molecules, including CO_2 and H_2O [51]. From the above analysis, it can be concluded that Fe_3Ce_1-HHTP has excellent SMX degradation property.

3.5. DFT calculations and degradation pathways

DFT calculation revealed the reaction sites where active species attacked SMX in heterogeneous EF process. The HOMO represented the position where electrons are easily detached, the LUMO represented the position where electrons are easily accessible, and the blue and green regions represented electron-rich and electron-poor regions, respectively (Fig. 9**a, b**) [52]. The optimized SMX molecular structure is shown in Fig. 9**c**. The ESP distribution map was computed to visualize density of electron cloud on SMX surface (Fig. 9**d**). To further locate atoms or groups that are more susceptible to attack, Hirshfeld charge and Fukui index (f^-, f^+, f^0, and CDD) were calculated and their structures are shown in Fig. 9**e-h**. Sites with high f^-, f^+ and f^0, values are theoretically the most susceptible to attacks from electrophilic, nucleophilic substances and free radicals [53]. CDD values were comprehensively considering the attack of nucleophilic and electricity. Due to the electrophilicity of ·OH, it can also undergo free radical reactions and electrophilic reactions [54]. **Table S3** exhibited that highest f^- and f^0 values is located at N11 (f^-=0.1851, f^0 = 0.1074), indicating that the vicinity of N11 was the most vulnerable site to be attacked by ·OH and $\cdot O_2^-$. The remaining atoms with higher f^- values appeared in C2, C4, C5, C6 and H12, and those with higher f^0 values were C1, C2, C3, C4, C6 and N11. In addition, atoms with higher f^- and f^0 values (C2, C4, C5, C6, N11) were mostly concentrated in the aniline group. Combined with images of Fukui function and calculation results, it was determined that C2, C4, C5, C6, and N11 were the main attack sites on aniline group of SMX. Additionally, N-C and S-N bonds of SMX exhibited a higher tendency to break.

To unequivocally elucidate degradation routes of SMX, various degradation intermediates were further identified through mass spectrometry. Fig. 10 depicted three SMX degradation pathways, the molecular formula, mass/charge ratio (m/z) and structures of SMX and intermediates are shown in **Table S4**. In pathway I, $–NH_2$ on benzene ring was initially oxidized by reactive oxygen species to $–NO_2$ to form P1 (m/z = 283). The formation of NH_4^+ was favored by the removal of nitrogen-containing compounds from benzene ring [55], thus the denitrification of P1 accelerated the generation of P2 (m/z = 238). The production of the intermediate P3 (m/z = 173) may be due to the Smiles rearrangement reaction [56]. In pathway II, SMX was directly cleaved at S-N bond, contributing to the formation of P4 (m/z = 157) and P5 (m/z = 98). Then, P6 (m/z = 114) was obtained by hydroxylation of P5. In pathway III, attacking on N-C bond within SMX molecule led to the production of P7 (m/z = 172). These were consistent with the active reaction sites obtained by DFT results. P4 then lost an amino group ($–NH_2$) and was further oxidized to form P8 (m/z = 142). These intermediates would continue to undergo oxidation by ·OH radicals, eventually resulting in the generation of P9 (m/z = 60), P10 (m/z = 72), and P11 (m/z = 89). Finally, these low molecular compounds are further broken down through ring breaking reaction and ultimately mineralized into CO_2, H_2O and inorganic ions.

3.6. Toxicity evaluation of SMX intermediates

The acute and growth toxicity levels of SMX and intermediates were predicted in Fig. 11. The acute toxicity was estimated to be LC_{50} for fathead minnow and IGC_{50} for T. pyriformis. The toxicity value of SMX

to fathead minnow was 2.81 mg/L, and the chronic toxicity value to T. pyriformis was 6.12 mg/L. As shown in Fig. 11**a**, except for P1 and P2, LC_{50} values were increased, indicating the toxicity of other intermediates was significantly reduced, especially P9 and P10, which were much lower than the toxicity of SMX and LC_{50} values were 4053.96 mg/L and 698.79 mg/L. For T. pyriformis (Fig. 11**b**), the concentration of P2 was lower than that of SMX, and the IGC_{50} values of the other intermediates were significantly higher than SMX, the IGC_{50} values of P6, P9, P10 and P11 were 1662.25 mg/L, 8931.38 mg/L, 3057.66 mg/L and 4178.46 mg/L, illustrating that heterogeneous EF system based on Fe_3Ce_1-HHTP catalyst can significantly reduce the acute toxicity of SMX. Fig. 11**c** showed the bioaccumulation factors for SMX and its intermediates. After EF treatment, only the bioaccumulation factor of P2 increased, indicating that it may be highly accumulated by aquatic organisms. As shown in Fig. 11**d**, although P1, P2, P3, P9, and P11 were considered "developmental toxicant", all intermediates had lower toxicity than SMX. Moreover, P4, P5, P6, P7, P8 and P10 were deemed as "developmental non-toxicant". The above results demonstrated that Fe_3Ce_1-HHTP catalyst is effective, environmentally friendly and promising for SMX degradation.

4. Conclusion

This study successfully synthesized Fe_3Ce_1-HHTP through a straightforward design strategy, serving as the efficient heterogeneous EF catalyst to degrade SMX. The synergistic effect of Fe and Ce improved heterogeneous EF performance of the Fe_3Ce_1-HHTP catalyst. Three-dimensional fluorescence spectrum could further prove the excellent degradation property. Furthermore, Fe_3Ce_1-HHTP catalyst showed good performance in wide pH range and exhibited satisfactory recyclability and stability after five cycles. The SMX degradation mechanism results demonstrated ·OH was the primary active species. According to DFT calculations and MS results, SMX formed eleven possible degradation intermediates products through three degradation pathways. Software prediction demonstrated that this heterogeneous EF system effectively reduced SMX biotoxicity. These findings offer significant insights for application of heterogeneous EF systems in the treatment of antibiotic wastewater.

CRediT authorship contribution statement

Shu-Ting Cheng: Writing – original draft, Methodology, Investigation, Formal analysis, Conceptualization. **Jia-Xin Song:** Methodology, Investigation, Formal analysis. **Li-Hong Yu:** Investigation, Formal analysis. **Xiao-Fang Shen:** Supervision, Project administration. **Yue-Hong Pang:** Writing – review & editing, Methodology, Funding acquisition.

Declaration of competing interest

The authors declare that they have no known competing financial interests or personal relationships that could have appeared to influence the work reported in this paper.

Data availability

Data will be made available on request.

Acknowledgements

This work was supported by the National Natural Science Foundation of China (22276077), and the Postgraduate Research & Practice Innovation Program of Jiangsu Province (KYCX23_2515).

Appendix A. Supplementary material

Supplementary data to this article can be found online at https://doi.org/10.1016/j.seppur.2024.128356.

References

[1] X. Zhang, D.D. Gang, J. Zhang, X. Lei, Q. Lian, W.E. Holmes, M.E. Zappi, H. Yao, Insight into the activation mechanisms of biochar by boric acid and its application for the removal of sulfamethoxazole, J. Hazard. Mater. 424 (2022) 127333, https://doi.org/10.1016/j.jhazmat.2021.127333.
[2] M. Ramya, P.S. Kumar, G. Rangasamy, V.U. Shankar, G. Rajesh, K. Nirmala, Experimental investigation of the electrochemical detection of sulfamethoxazole using copper oxide-MoS_2 modified glassy carbon electrodes, Environ. Res. 216 (2023) 114463, https://doi.org/10.1016/j.envres.2022.114463.
[3] X. Yi, C. Lin, E.J.L. Ong, M. Wang, Z. Zhou, Occurrence and distribution of trace levels of antibiotics in surface waters and soils driven by non-point source pollution and anthropogenic pressure, Chemosphere 216 (2019) 213–223, https://doi.org/10.1016/j.chemosphere.2018.10.087.
[4] S. Wang, X. Ma, Y. Liu, X. Yi, G. Du, J. Li, Fate of antibiotics, antibiotic-resistant bacteria, and cell-free antibiotic-resistant genes in full-scale membrane bioreactor wastewater treatment plants, Bioresource Technol. 302 (2020) 122825, https://doi.org/10.1016/j.biortech.2020.122825.
[5] L. Wang, H. Yang, M.H. Guo, Z. Wang, X. Zheng, Adsorption of antibiotics on different microplastics (MPs): Behavior and mechanism, Sci. Total Environ. 863 (2023) 161022, https://doi.org/10.1016/j.scitotenv.2022.161022.
[6] D. Li, W. Zhan, X. Gao, Q. Wang, L.P. Li, J. Zhang, G. Cai, W. Zuo, Y. Tian, Aminated waste paper membrane for efficient and rapid filtration of anionic dyes and antibiotics from water, Chem. Eng. J. 455 (2023) 140641, https://doi.org/10.1016/j.cej.2022.140641.
[7] X. Yuan, K. Cui, Y. Chen, S. Wu, X. Liu, H. Diao, Deciphering the response of biological nitrogen removal to gadolinium and sulfamethoxazole combined pollution: Performance, microbial community, and antibiotic resistance genes, Process Saf. Environ. 167 (2022) 192–202, https://doi.org/10.1016/j.psep.2022.09.030.
[8] R. Ren, X. Shang, Z. Song, C. Li, Z. Wang, F. Qi, A. Ikhlaq, J. Kumirska, E. Maria Siedlecka, O. Ismailova, Active electronic structure derived by Fe-Cl-C coordination of single-atom cathode applied in antibiotics degradation by electro-Fenton: Enhanced transformation of oxygen to hydroxyl radicals via 3-electron pathway, Chem. Eng. J. 474 (2023) 145545, 10.1016/j.cej.2023.145545.
[9] E. Liu, T. Hu, N.A. Al-Dhabi, T.O. Soyol-Erdene, O. Bayanjargal, Y. Zuo, J. Wang, W. Tang, MOF-derived Fe/Ni@C marigold-like nanosheets as heterogeneous electro-Fenton cathode for efficient antibiotic oxytetracycline degradation, Environ. Res. 247 (2024) 118357, https://doi.org/10.1016/j.envres.2024.118357.
[10] E. Mousset, W.H. Loh, W.S. Lim, L. Jarry, Z. Wang, O. Lefebvre, Cost comparison of advanced oxidation processes for wastewater treatment using accumulated oxygen-equivalent criteria, Water Res. 200 (2021) 117234, https://doi.org/10.1016/j.watres.2021.117234.
[11] Q. Yang, H. Mou, X. Hu, S. Qu, Y. Tsang, Study on the mechanisms of DMP degradation by electro-Fenton method modified by single atomic-Co doped carbon-based catalyst, Sep. Purif. Technol. 331 (2024) 125580, https://doi.org/10.1016/j.seppur.2023.125580.
[12] A. Xu, W. Liu, Z. Yang, L. Cao, I. Sirés, Q. Zhang, Y. Zhang, Waste tire upcycling for the efficient electrogeneration of H_2O_2 in advanced degradation of the antibiotic tinidazole by electro-Fenton process, J. Clean. Prod. 430 (2023) 139661, https://doi.org/10.1016/j.jclepro.2023.139661.
[13] D. Wang, Y. Li, S. Hu, J. Hu, H. Hou, B. Liu, H. Zheng, X. Luo, H. Li, A triple-cathode electron-Fenton system for efficient Fe^{2+} regeneration and in-situ H_2O_2 electro-activation, Sep. Purif. Technol. 299 (2022) 121704, https://doi.org/10.1016/j.seppur.2022.121704.
[14] H. Olvera-Vargas, J. Dubuc, Z. Wang, L. Coudert, C.M. Neculita, O. Lefebvre, Electro-fenton beyond the degradation of organics: Treatment of thiosalts in contaminated mine water, Environ. Sci. Technol. 55 (2021) 2564–2574, https://doi.org/10.1021/acs.est.0c06006.
[15] F.C. Moreira, R.A.R. Boaventura, E. Brillas, V.J.P. Vilar, Electrochemical advanced oxidation processes: A review on their application to synthetic and real wastewaters, Appl. Catal., b: Environ. (2017) 217–261, https://doi.org/10.1016/j.apcatb.2016.08.037.
[16] H. Olvera-Vargas, Z. Wang, J. Xu, O. Lefebvre, Synergistic degradation of GenX (hexafluoropropylene oxide dimer acid) by pairing graphene-coated Ni-foam and boron doped diamond electrodes, Chem. Eng. J. 430 (2022) 132686, https://doi.org/10.1016/j.cej.2021.132686.
[17] D. Yu, J. He, L. Bai, Y. Zheng, Z. Wang, O. Lefebvre, J. Zhang, High-valent metal-oxo species heterogeneous activation making use of MoS_2 in a novel electro-Fenton system: pH-independent catalytic environment and nonradical generation mechanism, Chem. Eng. J. 479 (2024) 147573, https://doi.org/10.1016/j.cej.2023.147573.
[18] Y. Li, B. Yao, Y. Chen, Y. Zhou, X. Duan, Metal-organic frameworks (MOFs) as efficient catalysts for electro-Fenton (EF) reactions: Current progress and prospects, Chem. Eng. J. 463 (2023) 142287, https://doi.org/10.1016/j.cej.2023.142287.
[19] X. Du, M. Zhou, Strategies to enhance catalytic performance of metal-organic frameworks in sulfate radical-based advanced oxidation processes for organic pollutants removal, Chem. Eng. J. 403 (2021) 126346, https://doi.org/10.1016/j.cej.2020.126346.

[20] H. Wang, C. Tang, L. Wang, Z. Sun, X. Hu, MOF-derived Co/Fe@NPC-500 with large amounts of low-valent metals as an electro-Fenton cathode for efficient degradation of ceftazidime, Appl. Catal., B: Environ. 333 (2023) 122755, 10.1016/j.apcatb.2023.122755.
[21] S. Cheng, C. Shen, H. Zheng, F. Liu, A. Li, OCNTs encapsulating Fe-Co PBA as efficient chainmail-like electrocatalyst for enhanced heterogeneous electro-Fenton reaction, Appl. Catal., b: Environ. (2020) 118785, https://doi.org/10.1016/j.apcatb.2020.118785.
[22] Y. Tian, X. Chen, X. Xing, Z. Li, X. Zhao, X. Lang, D. Yang, HHTP surface-functionalized copper sulfide hollow nanocubes with sensitivity-boosted and high-concentration ammonia sensing, Appl. Surf. Sci. 642 (2024) 158581, https://doi.org/10.1016/j.apsusc.2023.158581.
[23] X. Shi, R. Hua, Y. Xu, T. Liu, G. Lu, Trimetallic conductive metal-organic frameworks as precatalysts for the oxygen evolution reaction with enhanced activity, Sustain. Energ. Fuels 4 (2020) 4589–4597, https://doi.org/10.1039/d0se00515k.
[24] Y. Liu, H. Zhang, C. Yang, Z. Xu, Y. Shi, X. Zhu, X. Duan, L. Qin, Y. Jin, L. Song, M. Zhang, H. Zheng, Alkaline hydrogen production promoted by small-molecule modification on flowerlike $Co_2(OH)_2CO_3$, J. Energy Chem. 84 (2023) 73–80, https://doi.org/10.1016/j.jechem.2023.05.013.
[25] K.W. Nam, S.S. Park, R. dos Reis, V.P. Dravid, H. Kim, C.A. Mirkin, J.F. Stoddart, Conductive 2D metal-organic framework for high-performance cathodes in aqueous rechargeable zinc batteries, Nat. Commun. 10 (2019) 4948, https://doi.org/10.1038/s41467-019-12857-4.
[26] F. Wang, J. Hu, Y. Liu, G. Yuan, S. Zhang, L. Xu, H. Xue, H. Pang, Turning coordination environment of 2D nickel-based metal-organic frameworks by π-conjugated molecule for enhancing glucose electrochemical sensor performance, Mater. Today Chem. 24 (2022) 100885, https://doi.org/10.1016/j.mtchem.2022.100885.
[27] F. Gao, Y. Zhao, X. Dai, W. Xu, F. Zhan, Y. Liu, Q. Wang, Aptamer tuned nanozyme activity of nickel-metal–organic framework for sensitive electrochemical aptasensing of tetracycline residue, Food Chem. 430 (2024) 137041, https://doi.org/10.1016/j.foodchem.2023.137041.
[28] J. Dong, D.W. Boukhvalov, C. Lv, M.G. Humphrey, C. Zhang, Z. Huang, Enhancing the electrocatalytic activity of metal-organic frameworks in the oxygen evolution reaction by introducing high-valent metal centers, J. Mater. Chem. A 11 (2023) 16683–16694, https://doi.org/10.1039/d3ta01869e.
[29] X. Sun, Y. Li, H. Su, X. Zhang, Y. Xu, W. Zhou, M. Liu, W. Cheng, Q. Liu, Dissecting π-conjugated covalent-coupling over conductive MOFs toward efficient two-electron oxygen reduction, Appl. Catal., B: Environ. 317 (2022) 121706, 10.1016/j.apcatb.2022.121706.
[30] J. Li, Y. Huang, Y. Zhou, H. Dong, H. Wang, H. Shan, Y. Li, M. Xu, X. Wang, Controllable construction of two-dimensional conductive $M_3(HHTP)_2$ nanorods for electrochemical sensing of malachite green in fish, ACS Appl. Nano Mater. 6 (2023) 22916–22926, https://doi.org/10.1021/acsanm.3c04264.
[31] S.O. Ganiyu, M.J.G. de Araújo, E.C.T. de Araújo Costa, J.E.L. Santos, E.V. dos Santos, C.A. Martínez-Huitle, S.B.C. Pergher, Design of Highly Efficient Porous Carbon Foam Cathode for Electro-Fenton Degradation of Antimicrobial Sulfanilamide, Appl 119652 (2021) 283.
[32] Y. Dai, Y. Yao, M. Li, X. Fang, C. Shen, F. Li, Y. Liu, Carbon nanotube filter functionalized with MIL-101(Fe) for enhanced flow-through electro-Fenton, Environ. Res. 204 (2022) 112117, https://doi.org/10.1016/j.envres.2021.112117.
[33] Z. Li, C. Guo, J. Lyu, Z. Hu, M. Ge, Tetracycline degradation by persulfate activated with magnetic $Cu/CuFe_2O_4$ composite: Efficiency, stability, mechanism and degradation pathway, J. Hazard. Mater. 373 (2019) 85–96, https://doi.org/10.1016/j.jhazmat.2019.03.075.
[34] L. Qin, W. Chen, Y. Fu, J. Tang, H. Yi, L. Li, F. Xu, M. Zhang, W. Cao, D. Huang, C. Lai, Hemin derived iron and nitrogen-doped carbon as a novel heterogeneous electro-Fenton catalyst to efficiently degrade ciprofloxacin, Chem. Eng. J. 449 (2022) 137840, https://doi.org/10.1016/j.cej.2022.137840.
[35] P. Dong, H. Wang, W. Liu, S. Wang, Y. Wang, J. Zhang, F. Lin, Y. Wang, C. Zhao, X. Duan, S. Wang, H. Sun, Quasi-MOF derivative-based electrode for efficient electro-Fenton oxidation, J. Hazard. Mater. 401 (2021) 123423, https://doi.org/10.1016/j.jhazmat.2020.123423.
[36] M. Xu, J. Wei, X. Cui, J. Li, G. Pan, Y. Li, Z. Jiang, X. Niu, N. Cui, J. Li, High-efficiency electro-Fenton process based on in-situ grown CoFeCe-LDH@CFs free-standing cathodes: Correlation of cerium and oxygen vacancies with H_2O_2, Chem. Eng. J. 455 (2023) 140922, https://doi.org/10.1016/j.cej.2022.140922.
[37] X. Wang, Q. Zhang, J. Jing, G. Song, M. Zhou, Biomass derived S, N self-doped catalytic Janus cathode for flow-through metal-free electrochemical advanced oxidation process: Better removal efficiency and lower energy consumption under neutral conditions, Chem. Eng. J. 466 (2023) 143283, https://doi.org/10.1016/j.cej.2023.143283.
[38] H. Wu, W. Zhang, S. Kandambeth, O. Shekhah, M. Eddaoudi, H.N. Alshareef, Conductive metal–organic frameworks selectively grown on laser-scribed graphene for electrochemical microsupercapacitors, Adv. Energy Mater. 9 (2019) 1900482, https://doi.org/10.1002/aenm.201900482.
[39] X. Li, C. Xiao, X. Ruan, Y. Hu, C. Zhang, J. Cheng, Y. Chen, Enrofloxacin degradation in a heterogeneous electro-Fenton system using a tri-metal-carbon nanofibers composite cathode, Chem. Eng. J. 427 (2021) 130927, https://doi.org/10.1016/j.cej.2021.130927.
[40] Y. Chai, M. Bai, A. Chen, X. Xu, Z. Tong, J. Yuan, L. Peng, J. Shao, J. Xiong, C. Peng, Upcycling contaminated biomass into metal-supported heterogeneous catalyst for electro-Fenton degradation of thiamethoxam: Preparation, mechanisms, and implications, Chem. Eng. J. 453 (2023) 139814, https://doi.org/10.1016/j.cej.2022.139814.
[41] A. Huang, D. Zhi, H. Tang, L. Jiang, S. Luo, Y. Zhou, Effect of Fe^{2+}, Mn^{2+} catalysts on the performance of electro-Fenton degradation of antibiotic ciprofloxacin, and expanding the utilizing of acid mine drainage, Sci. Total Environ. 720 (2020) 137560, https://doi.org/10.1016/j.scitotenv.2020.137560.
[42] S. Han, Z. Wang, X. Pi, C. Wu, X. Wang, Y. Wang, X. Liu, H. Zhao, Promotion of tetracycline degradation by electro-Fenton: Controlling the reaction zone by N-doped modified activated carbon cathode, J. Clean Prod. 370 (2022) 133524, https://doi.org/10.1016/j.jclepro.2022.133524.
[43] J. Guo, G. Song, Y. Zheng, J. Gu, S. Li, M. Zhou, Single iron atoms embedded in MOF-derived nitrogen-doped carbon as an efficient heterogeneous electro-Fenton catalyst for degradation of carbamazepine over a wide pH, Sep. Purif. Technol. 302 (2022) 122141, https://doi.org/10.1016/j.seppur.2022.122141.
[44] P. Xia, Z. Ye, L. Zhao, Q. Xue, S. Lanzalaco, Q. He, X. Qi, I. Sirés, Tailoring single-atom FeN_4 moieties as a robust heterogeneous catalyst for high-performance electro-Fenton treatment of organic pollutants, Appl. Catal., B: Environ. 322 (2023) 122116, 10.1016/j.apcatb.2022.122116.
[45] H. Qi, X. Shi, Z. Liu, Z. Yan, Z. Sun, In situ etched graphite felt modified with $CuFe_2O_4/Cu_2O/Cu$ catalyst derived from CuFe PBA for the efficient removal of sulfamethoxazole through a heterogeneous electro-Fenton process, Appl. Catal., B: Environ. 331 (2023) 122722, 10.1016/j.apcatb.2023.122722.
[46] X. Chen, W. Teng, J. Fan, Y. Chen, Q. Ma, Y. Xue, C. Zhang, W. Zhang, Enhanced degradation of micropollutants over iron-based electro-Fenton catalyst: Cobalt as an electron modulator in mesochannels and mechanism insight, J. Hazard. Mater. 427 (2022) 127896, https://doi.org/10.1016/j.jhazmat.2021.127896.
[47] J. Lou, J. An, X. Wang, M. Cheng, Y. Cui, A novel DBD/VUV/PMS process for efficient sulfadiazine degradation in wastewater: Singlet oxygen-dominated nonradical oxidation, J. Hazard. Mater. 461 (2024) 132650, https://doi.org/10.1016/j.jhazmat.2023.132650.
[48] J. Zhang, D. Wang, F. Zhao, J. Feng, H. Feng, J. Luo, W. Tang, Ferrate modified carbon felt as excellent heterogeneous electro-Fenton cathode for chloramphenicol degradation, Water Res. 227 (2022) 119324, https://doi.org/10.1016/j.watres.2022.119324.
[49] X. Zhang, B. Xu, S. Wang, X. Li, C. Wang, B. Liu, F. Han, Y. Xu, P. Yu, Y. Sun, Tetracycline degradation by peroxymonosulfate activated with CoNx active sites: Performance and activation mechanism, Chem. Eng. J. 431 (2022) 133477, https://doi.org/10.1016/j.cej.2021.133477.
[50] X. Gao, H. Zhang, Y. Wang, H. Wang, Y. Tang, Y. Hu, Y. Lv, J. Bai, Study on preparation of a novel needle coke heterogeneous electro-Fenton cathode for coking wastewater treatment, Chem. Eng. J. 455 (2023) 140696, https://doi.org/10.1016/j.cej.2022.140696.
[51] Y. Wu, J. Chen, H. Che, X. Gao, Y. Ao, P. Wang, Boosting $2e^-$ oxygen reduction reaction in garland carbon nitride with carbon defects for high-efficient photocatalysis-self-Fenton degradation of 2,4-dichlorophenol, Appl. Catal., B: Environ. 307 (2022) 121185, 10.1016/j.apcatb.2022.121185.
[52] Y. Liu, S. Liu, M. Chen, Y. Bai, Y. Liu, J. Mei, B. Lai, Enhanced TC degradation by persulfate activation with carbon-coated $CuFe_2O_4$: The radical and non-radical co-dominant mechanism, DFT calculations and toxicity evaluation, J. Hazard. Mater. 461 (2024) 132417, https://doi.org/10.1016/j.jhazmat.2023.132417.
[53] Y. Yu, C. Yu, Z. Wu, B. Huang, P. Zhou, H. Zhang, W. Liu, Y. Liu, Z. Xiong, B. Lai, Switching the primary mechanism from a radical to a nonradical pathway in electrocatalytic ozonation by onsite alternating anode and cathode, Chem. Eng. J. 457 (2023) 141340, https://doi.org/10.1016/j.cej.2023.141340.
[54] L. Lai, H. Ji, H. Zhang, R. Liu, C. Zhou, W. Liu, Z. Ao, N. Li, C. Liu, G. Yao, B. Lai, Activation of peroxydisulfate by V-Fe concentrate ore for enhanced degradation of carbamazepine: Surface ≡V(III) and ≡V(IV) as electron donors promoted the regeneration of ≡Fe(II), Appl. Catal., B: Environ. 282 (2021) 119559, 10.1016/j.apcatb.2020.119559.
[55] D. Liu, D. Chen, L. Jiang, Z. Hao, R. Tan, B. Deng, Y. Wang, Y. Tian, L. Chen, B. Jia, Efficient degradation of sulfamethoxazole in heterogeneous Electro-Fenton process with CeO_2@MoS_2@GF modified cathode: Mechanism and degradation pathway, Sep. Purif. Technol. 320 (2023) 124212, https://doi.org/10.1016/j.seppur.2023.124212.
[56] J. Hou, J. Wan, Z. Yan, Y. Wang, Y. Ma, Y. Xie, H. Chen, Y. Xue, A novel polydopamine-modified metal organic frameworks catalyst with enhanced catalytic performance for efficient degradation of sulfamethoxazole in wastewater, Chemosphere 297 (2022) 134100, https://doi.org/10.1016/j.chemosphere.2022.134100.